Photochromic and luminescent compounds as artificial neuron models.

Pier Luigi Gentili,[1,*] Maria Sole Giubila,[1] Raimondo Germani,[1] B. Mark Heron.[2]

[1] Department of Chemistry, Biology and Biotechnology, University of Perugia, 06123 Perugia, Italy

[2] Department of Chemical and Biological Sciences, School of Applied Science, University of Huddersfield, Queensgate, Huddersfield, HD1 3DH, UK

* Corresponding author Fax: (+39) 075-585-5598; Tel: (+39) 075-585-5573; E-mail: pierluigi.gentili@unipg.it

Abstract

This work is an important contribution to the development of neuromorphic engineering based on solutions of nonlinear chemical systems. It reports the results of experiments and simulations regarding the optical communication between the Belousov-Zhabotinsky reaction and photochromic and luminescent materials. It demonstrates that thermally reversible photochromic and luminescent compounds are dynamic models of phasic photo-excitable neurons. Moreover, it shows that photo-reversible photochromic compounds can be used for the implementation of optical synapsis and memory effects. Finally, it reports the first example of transmission of a chaotic signal between a Hydrodynamic Photochemical Oscillator based on a photochromic naphthopyran and a luminescent acridinium salt.

Keywords: Photochromism; Luminescence; Optical Communication; Synchronization; Chaos.

1.Introduction

Artificial intelligence is having an enormous impact on our societies because it is becoming ubiquitous in our daily lives as well as in industry and fundamental research. There are two main strategies to develop artificial intelligence: one is writing human-like intelligent programs running on computers or special-purpose hardware [1], and the other is neuromorphic engineering [2]. Neuromorphic engineering implements surrogates of neurons through non-biological systems either for neuro-prosthesis [3] or to devise brain-like computing machines. Brain-like computing machines will exhibit the peculiar performances of human intelligence, such as learning, recognizing variable patterns and computing with words as some programs have commenced doing. However, it is expected that brain-like computers will have the advantage of requiring much less power and occupying much less space than our best electronic supercomputers. Surrogates of neurons for brain-like computers can be implemented by using different strategies. One strategy consists of using conventional passive and active circuit elements, either analog [2, 4] or digital [5]. Another approach is to design circuits containing two-terminal devices with multiply-valued internal states that can be tuned in non-volatile or quasi-stable manners, mimicking synaptic interconnections [6-8]. There is also the possibility of using phase-change devices wherein the actual membrane potential of the artificial neuron is stored in the form of the phase configuration of a chalcogenide-based material, which can undergo phase transition on a nanosecond timescale and at the nanometric level [9]. Finally, there is the strategy of devising brain-like computing machines based on wetware rather than hardware, by using solutions of nonlinear chemical systems [10-13]. This work is a contribution to the development of this latter strategy.

Neurons are nonlinear dynamic systems that communicate reciprocally and develop rhythmic activity [14, 15]. Therefore, to mimic the behavior of neurons, it is useful to implement and study the synchronization of nonlinear chemical systems. It has been shown that nonlinear chemical systems can communicate through either continuous mass exchange [16], or electrochemical linkages [17,

18], or mechanical/light-induced pulsed release of chemicals [19, 20-22]. Recently, in our group, we have proposed the use of UV-visible radiation as excitatory and inhibitory optical signals that allow synchronizing oscillatory chemical reactions and photo-excitable chemical systems [23]. In this paper, we present, through experiments and simulations, the usefulness of photochromic and luminescent compounds in the implementation of artificial neural networks where UV and visible radiation are used as signals. With respect to our first publication [23], we demonstrate that thermally reversible photochromic and luminescent compounds are dynamic models of phasic photo-excitable neurons. Moreover, we show that photo-reversible photochromic compounds can be used for the implementation of optical synapsis and memory effects. Finally, we propose the use of the Hydrodynamic Photochemical Oscillator as a dynamic model of a chaotic neuron, and we report the first example of transmission of a chaotic optical signal. The compounds used in this work are shown in Scheme 1. They are three thermally reversible (T-type) photochromic compounds, *i.e.*, one spirooxazine (**SpO**) and two naphthopyrans (**MeOPh**, **MPh**); azobenzene (**Azo**) that is both a photo- and thermo-reversible photochromic molecule; one diarylethene (**DTEB**) that is a photo-reversible photochromic compound, and, finally, one fluorescent acridinium salt (**C_8Ac**). The Belousov-Zhabotinsky reaction with cerium as the catalyst has been used as a model of a pacemaker neuron communicating with photochromic and luminescent compounds through UV signals.

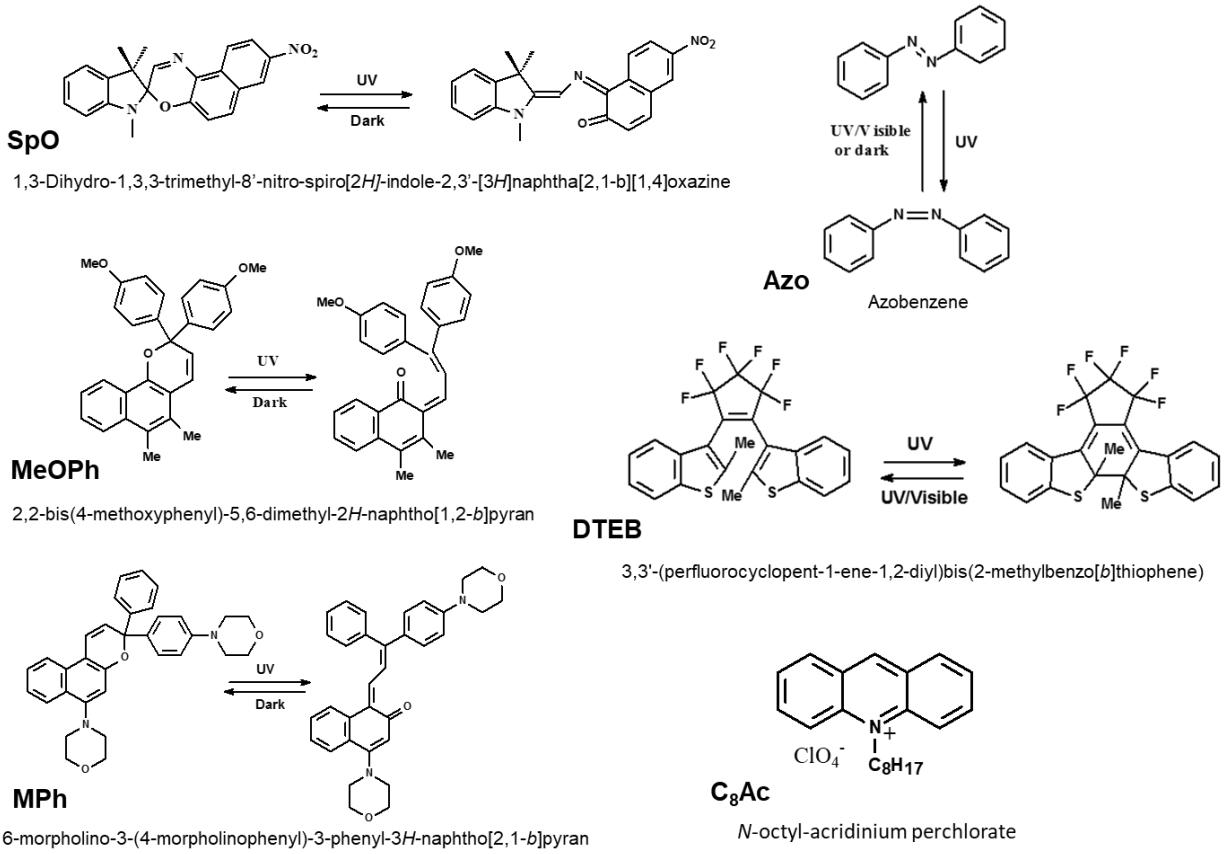

Scheme 1. Structures and names of the photochromic and fluorescent compounds used in this work.

2.Experimental

2.1 Materials, facilities and experimental methods

Deionized water, acetonitrile (from Fluka, ≥99.8%) and acetone (from Sigma-Aldrich) were used as solvents. Acetone was distilled before use. The chemicals used to carry out the Belousov-Zhabotinsky reactions were malonic acid (99+%, Carlo Erba), $NaBrO_3$ (99.5%, Alfa Aesar), H_2SO_4 (96%, Panreac), and ceric sulfate (98+%, Carlo Erba) as the catalyst. The compound 1,3-Dihydro-1,3,3-trimethyl-8′-nitro-spiro[2*H*-indole-2,3′-[3*H*]naphth[2,1-*b*][1,4]oxazine] (**SpO**) was supplied by Great Lakes Chemical Italia S.r.l.; Azobenze (**Azo**) was purchased from Fluka (≥ 97%); 6-morpholino-3-(4-morpholinophenyl)-3-phenyl-3*H*-naphtho[2,1-*b*]pyran (**MPh**) and 2,2-bis(4-methoxyphenyl)-5,6-dimethyl-2*H*-naphtho[1,2-*b*]pyran (**MeOPh**) were synthesized according to the procedure published in reference [24]; 3,3'-(perfluorocyclopent-1-ene-1,2-

diyl)bis(2methylbenzo[*b*]thiophene) (**DTEB**) was synthesized according to the procedure published in reference [25]; *N*-octyl-acridinium perchlorate (**C_8Ac**) was synthesized according to the procedure published in reference [23].

For the investigation of the optical communication between two artificial neuron models, located into two distinct cuvettes, an AvaSpec-ULS2048-2-USB2 Dual Channel Ultra-low straylight Fiber Optic Spectrometer equipped with 75 mm Avabench, 2048-pixel CCD detector, 2 x USB powered high-speed USB2 interface, 2xUSB cable, and sync cable was used. The spectrophotometer operates in the range 200-800 nm. The radiation emitted by a Deuterium-Halogen light source was conveyed to the two solutions through a 200 μm bifurcated optical fiber. The UV-visible radiation either transmitted or emitted by the two cuvettes was collected by two distinct 200 μm optical fibers and conveyed to the 2048-pixel CCD detector. The radiation emitted by the lamp of the spectrophotometer and those emitted or transmitted by the samples were focused by some collimating lens.

The irradiation intensity was determined by performing spectro-radiometric measurements. An irradiance-calibrated AvaSpec-2048-2 spectrometer (Avantes, NL) provided with a 200-micrometer diameter optical fiber (FC-UVIR200-2ME, Avantes) and an 8-mm active area cosine corrector (CC-UV- VIS/NIR, Avantes) was used. The spectro-radiometer operates in the 171–1100 nm range (300 lines per mm grating) and is equipped with an AvaBench-75 optical bench, a 25-micrometer slit which produced 1.2 nm FWHM spectral resolution and a 2048-pixel CCD detector.

All the experiments were repeated at least twice and were carried out at room temperature, with the samples equilibrated with air. The Belousov-Zhabotinsky reactions were always performed inside cuvettes and under magnetic stirring.

2.2 Computational methods

The experimental results of synchronization between pairs of artificial neuron models and memory effects have been reproduced and interpreted by formulating non-linear differential

equations and solving them through numerical integration with the solver ode45 implemented in MATLAB.

The features of chaotic time series, each containing N=1750 data, $A^* = \{A_i, i = 1, \dots, N\}$, have been investigated by using the TISEAN code [26]. First, the phase spaces of the time series have been built by using the Takens' time-delay embedding theorem [27]. According to the Takens' theorem, the reconstruction of the phase space requires the determination of the time delay (τ) and the embedding dimension (*m*). Then, the chaotic characters of the time series have been investigated by calculating the largest Lyapunov exponent (λ) and the correlation dimension (D) of the time series plotted in their phase spaces.

The time delays have been determined by calculating the mutual information S(τ) [28]:

$$S(\tau) = -\sum_{ij} p_{ij}(\tau) ln \frac{p_{ij}(\tau)}{p_i p_j} \quad (1)$$

where for some partition on the real numbers, p_i is the probability of finding a time series value in the *i'*th interval, and $p_{ij}(\tau)$ is the joint probability that an observation falls in the *i'*th interval and at the observation time τ later falls into the *j'*th one. A good estimate of τ is the first local minimum of S(τ).

The embedding dimensions (*m*) have been estimated by the false nearest neighbor method [29]. The original time series *A** have been transformed into matrices whose elements are a time-lagged version of the data. One example of these matrices is shown in (2):

$$\boldsymbol{A} = \begin{pmatrix} A_1 & A_{1+\tau} & & A_{1+(m-1)\tau} \\ A_2 & A_{2+\tau} & & A_{2+(m-1)\tau} \\ . & . & \dots & . \\ A_{N-(m-1)\tau} & A_{N-(m-2)\tau} & & A_N \end{pmatrix} = \begin{pmatrix} \bar{A}_1 \\ \bar{A}_2 \\ . \\ \bar{A}_{N-(m-1)\tau} \end{pmatrix} \quad (2)$$

For each point $\bar{A}_i$ in the *m*-dimensional phase space, the method looks for its nearest neighbor $\bar{A}_j$. It calculates the square of the Euclidean distance

$$R^2_{m,i} = \sum_{k=0}^{m-1} \left(A_{i+k\tau} - A_{j+k\tau}\right)^2 \quad (3)$$

In going from dimension *m* to dimension *m+1* by time delay embedding we add a (*m+1*)'th coordinate onto each of the vectors, $\bar{A}_i$ and $\bar{A}_j$. After the addition of the new (*m+1*)'th coordinate, the distance between $\bar{A}_i$ and $\bar{A}_j$ is

$$R_{m+1,i}^2 = R_{m,i}^2 + \left(A_{i+m\tau} - A_{j+m\tau}\right)^2 \quad (4)$$

We designate as a false neighbor any neighbor for which

$$\left(\frac{R_{m+1,i}^2 - R_{m,i}^2}{R_{m,i}^2}\right)^{1/2} = \frac{\left|A_{i+m\tau} - A_{j+m\tau}\right|}{R_{m,i}} > R_t \quad (5)$$

where R_t is a given heuristic threshold. When the number of false neighbors is zero, *m* is the suitable embedding dimension.

The largest Lyapunov exponents have been calculated by the Rosenstein's algorithm [30]. Rosenstein's method locates the nearest neighbor of each point after reconstructing the phase space. The nearest neighbor, $\bar{A}_{\hat{j}}$, is found by searching for the point that minimizes the initial distance to the particular reference point $\bar{A}_j$. This distance is expressed as

$$d_j(0) = \min_{\bar{A}_{\hat{j}}} \left\| \bar{A}_j - \bar{A}_{\hat{j}} \right\| \quad (6)$$

where $\| \quad \|$ denotes the Euclidean norm. From the definition of the Lyapunov exponent, the *j'*th pair of nearest neighbors diverge approximately at a rate given by the largest Lyapunov exponent after *i* discrete time steps (*i.e.*, after a time $i\Delta t$, where Δt is the sampling period of the time series):

$$d_j(i) \approx d_j(0) e^{\lambda_1 (i\Delta t)} \quad (7)$$

In logarithmic form, equation (7) becomes

$$ln\left(d_j(i)\right) = ln\left(d_j(0)\right) + \lambda_1 (i\Delta t) \quad (8)$$

The linear relation (8) can be determined for each point in the phase space. The largest Lyapunov exponent is calculated using a least-squares fit to the "average" line defined by

$$y(i) = \frac{1}{\Delta t}\langle lnd_j(i)\rangle \quad (9)$$

where the average is carried out over all values of j.

The strangeness of attractors has been measured by determining the correlation dimensions D with the Grassberger-Procaccia algorithm [31], which requires calculation of the correlation sum:

$$C(m,\varepsilon) = \frac{1}{N'^2}\sum_{i\neq j}^{N'} \Theta(\varepsilon - \left\|\bar{A}_i - \bar{A}_j\right\|) \quad (10)$$

where ε is the size of the cell (whose minimum is given by data interval/1000 and whose maximum is the data interval), $N' = N - \tau(m-1)$, and Θ is the Heaviside step function, which is 1 when $\left\|\bar{A}_i - \bar{A}_j\right\| \leq \varepsilon$, whereas it is 0 when $\left\|\bar{A}_i - \bar{A}_j\right\| > \varepsilon$. Then, the correlation sum is exploited to measure the correlation dimension, assuming that

$$C(m,\varepsilon) \propto \varepsilon^D \quad (11)$$

In practice, one looks for convergence of the estimated values of D as a function of the embedding dimension m.

3.Results

Human intelligence emerges from the complex structural and dynamic properties of our nervous system. The primary cellular elements of our nervous systems are neurons. The computational power of neurons relies on their dynamic properties. Every neuron is a nonlinear dynamic system [14, 15]. Neurons can be grouped into three sets if we focus on their nonlinear dynamic properties.

A first set includes neurons that are in the oscillatory regime. They are called pacemaker neurons and fire action potentials periodically. Pacemaker neurons generate rhythmic activities in neural networks involved in the neocortex, basal ganglia, thalamus, locus coeruleus, hypothalamus, ventral tegmentum area, hippocampus and amygdala [32]. These structures are associated with sleep, wakefulness, arousal, motivation, addiction, memory consolidation, cognition, and fear.

A second set includes excitable neurons. There are "tonic" excitable neurons that respond to a constant excitatory signal by firing a sequence of spikes. But, there are also "phasic" excitable neurons that respond to an excitatory stimulus firing just once. "Tonic" excitable neurons are, for example, in the cortex. "Phasic" excitable neurons are, for example, in auditory brainstem (involved in precise timing computations) and in the spinal cord [33, 34].

Finally, the third set includes chaotic neurons. Chaotic neurons are quite common in the nervous system because the intrinsic dynamic instability facilitates the extraordinary ability of neural networks to adapt [15, 35].

The computational power of neural networks relies on the synchronization among neurons, which depends on the synaptic interconnections that are adjustable and non-volatile [15].

We have proposed the use of oscillatory chemical reactions as models of the dynamics of pacemaker neurons [12, 20, 23]. For example, the Belousov-Zhabotinsky reaction (**BZ**), carried out under cerium ion catalysis, gives rise to significant transmittance oscillations in the UV part of the electromagnetic spectrum. If a UV radiation with constant intensity crosses the **BZ** reaction, its intensity is modulated. The **BZ** reaction transmits a UV ray, whose intensity oscillates, and the frequency of oscillations coincides with the intrinsic frequency of the **BZ** [23].

Phasic photo-excitable artificial neuron models

We propose the use of direct thermally reversible photochromic compounds as dynamic models of "phasic" excitable neurons sensitive to UV signals. In fact, they respond to a steady UV signal, by coloring and reaching a stable photo-stationary state. Moreover, they "relax", *i.e.*, they recover the initial colorless state, as soon as the UV signal is discontinued. In other words, a direct thermally reversible photochromic compound fires a pseudo-action potential just once upon steady UV irradiation. On the other hand, if it receives a periodic excitatory UV signal, it tends to synchronize

with it. For example, if the photo-excitable **MeOPh** receives a periodic UV signal transmitted by an oscillatory **BZ** reaction taking place in another cuvette, as shown in Figure 1A, we can observe a phenomenon of synchronization. The UV signal transmitted by the **BZ** reaction is excitatory for **MeOPh**. The pink colour is generated in the solution of **MeOPh** due to the ring-opened form of the photochromic compound (see the spectra in Figure 1B). The saturation of the pink colour oscillates. The amplitude of the absorbance oscillations depends on the concentration of the photochromic compound and the intensity of the UV signal. The larger the UV transmittance of the **BZ**, the stronger the saturation of the pink colour. The **BZ** and **MeOPh** synchronize out-of-phase due to the relatively slow response of the photochromic compound (see Figure 1C). The phase difference is ~55° as shown in Figure S1 in the Supporting Information (SI). The differential equation describing the synchronization (see paragraph 2 in SI) has been solved by numerical integration. It reveals that the phase difference ($\Delta\theta$) between the oscillatory **BZ** and a direct thermally reversible photochromic compound depends on the lifetime of the coloured form: the longer the lifetime, the larger the phase difference (see Figure S2). As soon as the **BZ** reaction stops to send excitatory signals to **MeOPh**, the photochromic species ceases to oscillate and recovers its initial uncolored state, as required to a "phasic" photo-excitable artificial neural model. An optical-based "master-and-slave" relationship is established between the **BZ** reaction and **MeOPh**.

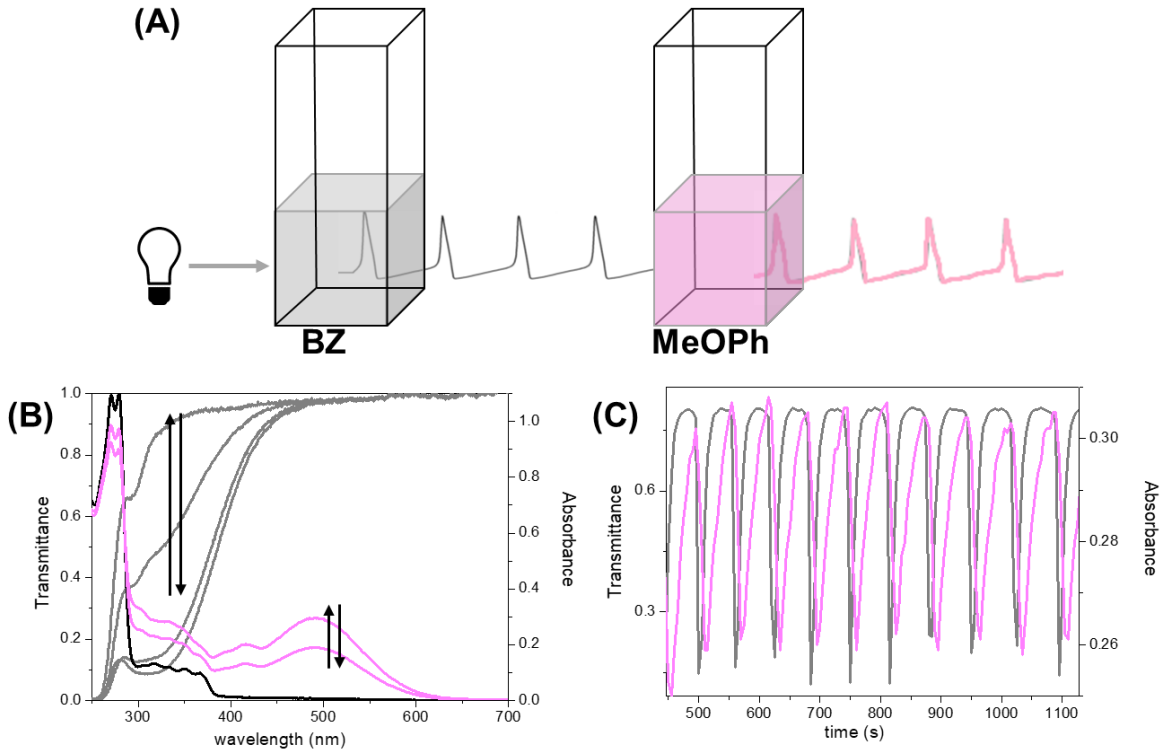

Figure 1. (A) Scheme of the optical communication between **BZ** and **MeOPh**. The initial concentrations of the **BZ** reagents are: $[NaBrO_3]_0$=0.058 M, $[CH_2(COOH)_2]_0$=0.2 M, $[Ce(SO_4)_2]_0$=0.003 M, $[H_2SO_4]_0$=0.51 M. **MeOPh** is dissolved in acetonitrile at the concentration of 0.0001 M. (B) Four representative transmittance spectra of the **BZ** (in grey) and absorption spectra of the uncolored (black) and colored forms (pink spectra) of **MeOPh**. (C) Time evolutions of the transmittance of **BZ** at 320 nm (grey trace) and the absorbance of **MeOPh** at 493 nm (pink trace).

A "one-master-and-two-slaves" relationship can be established when the **BZ** reaction transmits an excitatory periodic UV signal to a cuvette containing a solution of two distinct thermally reversible photochromic compounds, such as **MPh** and **SpO**. The spectral properties of the uncolored (Un) and colored (Co) forms of both photochromic species are shown in Figure 2A. **MPh** and **SpO** compete spectroscopically in capturing the excitatory UV signal transmitted by the **BZ**. The spectral evolution associated with the photochemical reactions Un→Co of both photochromic compounds influences the reciprocal optical actions between **MPh** and **SpO**. For example, at 308 nm that is the wavelength

transmitted by the **BZ** in the experiment, the absorption coefficient of Un(**SpO**), $\varepsilon_{Un}(\mathbf{SpO}) = 22100\ M^{-1}cm^{-1}$, is much larger than that of Co(**SpO**), $\varepsilon_{Co}(\mathbf{SpO}) = 5400\ M^{-1}cm^{-1}$ ($\varepsilon_{Un}(\mathbf{SpO}) > \varepsilon_{Co}(\mathbf{SpO})$) (see the arrows in Figure 2A). Therefore, the transformation of the reagent Un(**SpO**) into the product Co(**SpO**) exerts a positive self-feedback action on its coloration (because the larger the Co concentration, the more probable the absorption by the remaining Un molecules) and an excitatory action on the photo-coloration of **MPh**. On the other hand, $\varepsilon_{Un}(\mathbf{MPh}) = 7300\ M^{-1}cm^{-1} < \varepsilon_{Co}(\mathbf{MPh}) = 10540 M^{-1}cm^{-1}$. Hence, the transformation of the reagent Un(**MPh**) into the product Co(**MPh**) exerts a negative self-feedback action on its coloration and an inhibitory action on the photo-coloration of **SpO**. The inherent spectral features of the two photochromic compounds allow implementing a recurrent network (**RN₁**) with the feedback actions schematically depicted in Figure 2B (the excitatory and inhibitory actions are represented by arrows and flattened arrowheads, respectively). The development of a kinetic model for the recurrent network **RN₁** (see paragraph 3 in the SI) allows confirming the reciprocal spectroscopic action exerted between **MPh** and **SpO**. In fact, the top layer of Figure 2C shows that the concentration of Co(**SpO**) would be larger without the negative feedback action played by **MPh** (red trace respect to the black trace) and it would be smaller without its positive autaptic (*i.e.*, self-feedback) action (blue trace). On the other hand, the bottom layer of the graph (C) in Figure 2 demonstrates that the concentration of Co(**MPh**) would be smaller without the positive feedback action exerted by **SpO** (red trace instead of the black one), whereas it would be larger without its negative autaptic action (blue trace). Independently of the mutual spectroscopic influence, both **MPh** and **SpO** synchronize out-of-phase with the **BZ** reaction. Since Co(**MPh**) and Co(**SpO**) have similar lifetimes (*i.e.*, ~38 s), the two photochromic compounds show the same phase difference ($\Delta\theta$~70°). Therefore, they are mutually in-phase, as it can be inferred by looking at the experimental results shown in Figure 2D where the blue and red traces refer to the absorbances recorded at 611 nm and 488 nm, which are the maxima of the bands in the visible region generated by Co(**SpO**) and Co(**MPh**), respectively.

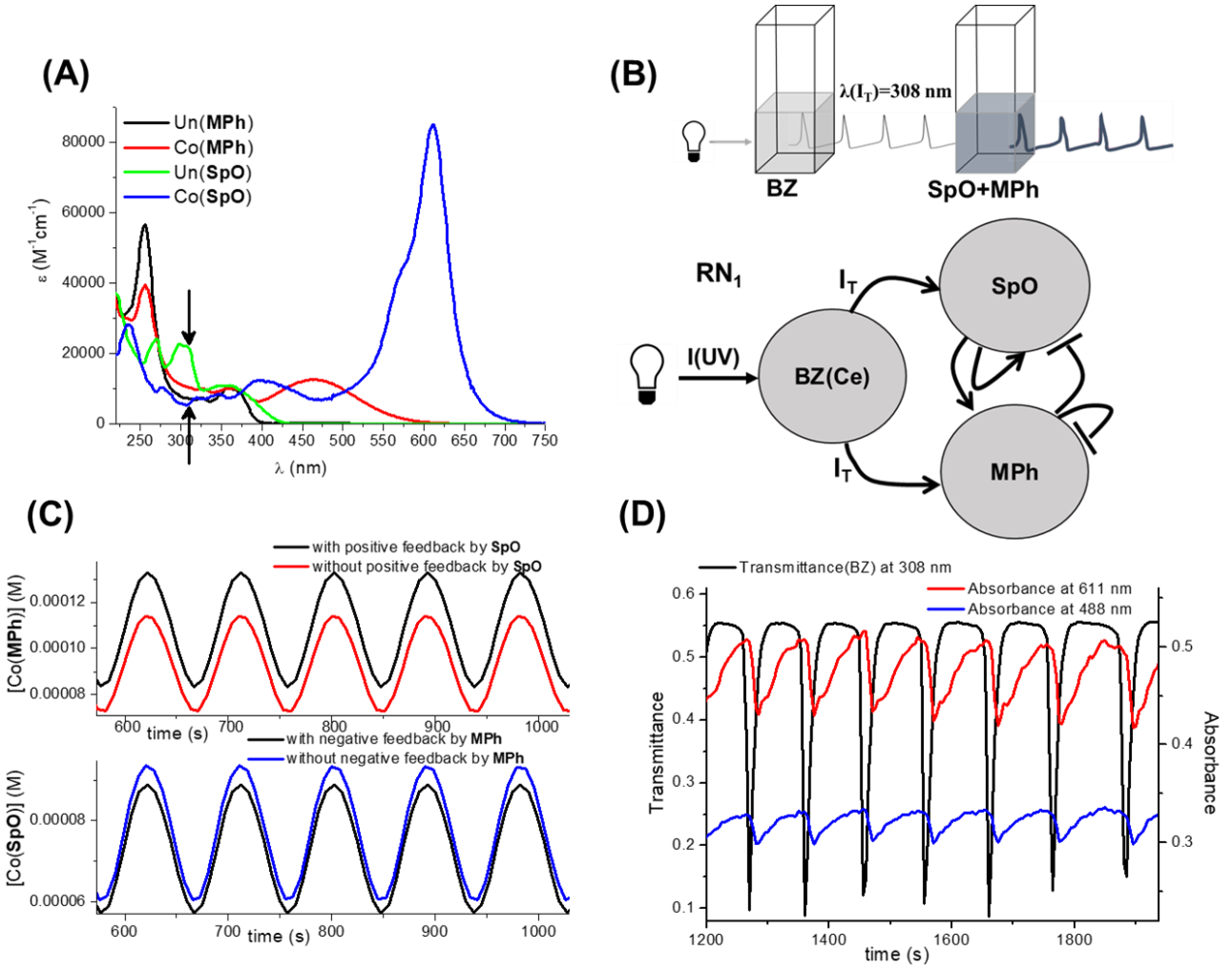

Figure 2. Spectral properties of uncolored (Un) and colored (Co) forms of **MPh** and **SpO** in graph A; schematic structure of the recurrent network **RN₁** in graph B under the assumption that the UV signal transmitted by **BZ** is at 308 nm (**SpO** and **MPh** are in the same cuvette); simulation of the inhibitory action of **MPh** and the excitatory autaptic action of **SpO** on its colouration (top layer in graph C); simulation of the excitatory action of **SpO** and the inhibitory autaptic action of **MPh** on its colouration (bottom layer in graph C); out-of-phase synchronization between the UV intensity transmitted by **BZ** and the absorbance signals at 611 nm that is the maximum of the absorption for Co(**SpO**), and at 488 nm that is the maximum of the absorption for Co(**MPh**).

Memory effects

Memory is a relevant function of our brain. By learning and retaining information, we filter the flood of data that confront us on a daily basis, avoiding information overloads and keeping us sane. Following Hebb's ideas, most studies of the mechanisms underlying learning and memory focus on changing the efficacy of synaptic connections [15]. The efficacy of synaptic transmission is activity-dependent and continuously modified. Examples of such modifications are long-term potentiation (LTP) and depression (LTD), which consists in increasing or decreasing conductivity, respectively, of synaptic connections between two neurons, leading to increased or decreased activity over time.

In our project of developing artificial neural models communicating through UV and visible radiation, we propose the use of photo-reversible photochromic compounds for the implementation of memory effects and adjustable optical synaptic connections.

An example is shown in Figure 3 where simulated data are reported. The simulations avoid a flattening of the spectra in the UV region in the case of high absorbance values and the possibility of discriminating the spectral and dynamic contributions of the different components of a mixture. Figure 3A reports the spectral response of a solution containing **MPh** alone ([Un(**MPh**)]=0.00025 M) to the periodic signal transmitted by **BZ**. Before excitation, **MPh** absorbs only in the UV (black spectrum). When excited for a while by the oscillatory UV signal transmitted by the **BZ** reaction, the spectrum of **MPh** oscillates between the blue and red traces, determining an oscillation in the saturation of the orange color. When the excitation stops, **MPh** ceases the oscillations, and the Co(**MPh**) transforms back to the original Un(**MPh**) completely, and in about one minute (in fact, the bleaching kinetic constant of Co(**MPh)** is $k_{\Delta} = 0.027s^{-1}$). Any trace of the previous excitation disappears. The system does not have any memory of what happened before.

If we introduce the photo-reversible photochromic diarylethene **DTEB** into the solution of **MPh**, we can implement a memory effect. In fact, before any UV and visible excitation, the system with **MPh** (0.00025 M) and **DTEB** (0.00005 M) absorbs only in the UV (black trace in Figure 3B). Upon

oscillatory UV excitation, the uncolored forms of both **DTEB** and **MPh** transform into the respective colored forms. Whereas the concentration of Co(**MPh**) oscillates (blue trace of Figure 3C), that of Co(**DTEB**) grows exponentially up to reach a photo-stationary state (red trace of Figure 3C). The sum $[\mathrm{Co}(\mathbf{MPh})] + [\mathrm{Co}(\mathbf{DTEB})]$ oscillates (black trace of Figure 3C) and, after about 600 s, the spectra we record are included between the limit blue and red traces shown in Figure 3B. If we discontinue the UV excitation, Co(**MPh**) disappears, but Co(**DTEB**) remains indefinitely (see the green trace of Figure 3B), exerting a memory effect. Since the absorbance of the system Un(**MPh)**+Co(**DTEB**) is everywhere larger than that of the system with **MPh** alone (compare the spectra of Figure 3B), the presence of Co(**DTEB**) guarantees a sort of long-term potentiation of the absorbance values of the photochromic solution, in both the UV and visible region (see also paragraphs 4a and 4b in SI for the details of the simulations and the experimental results).

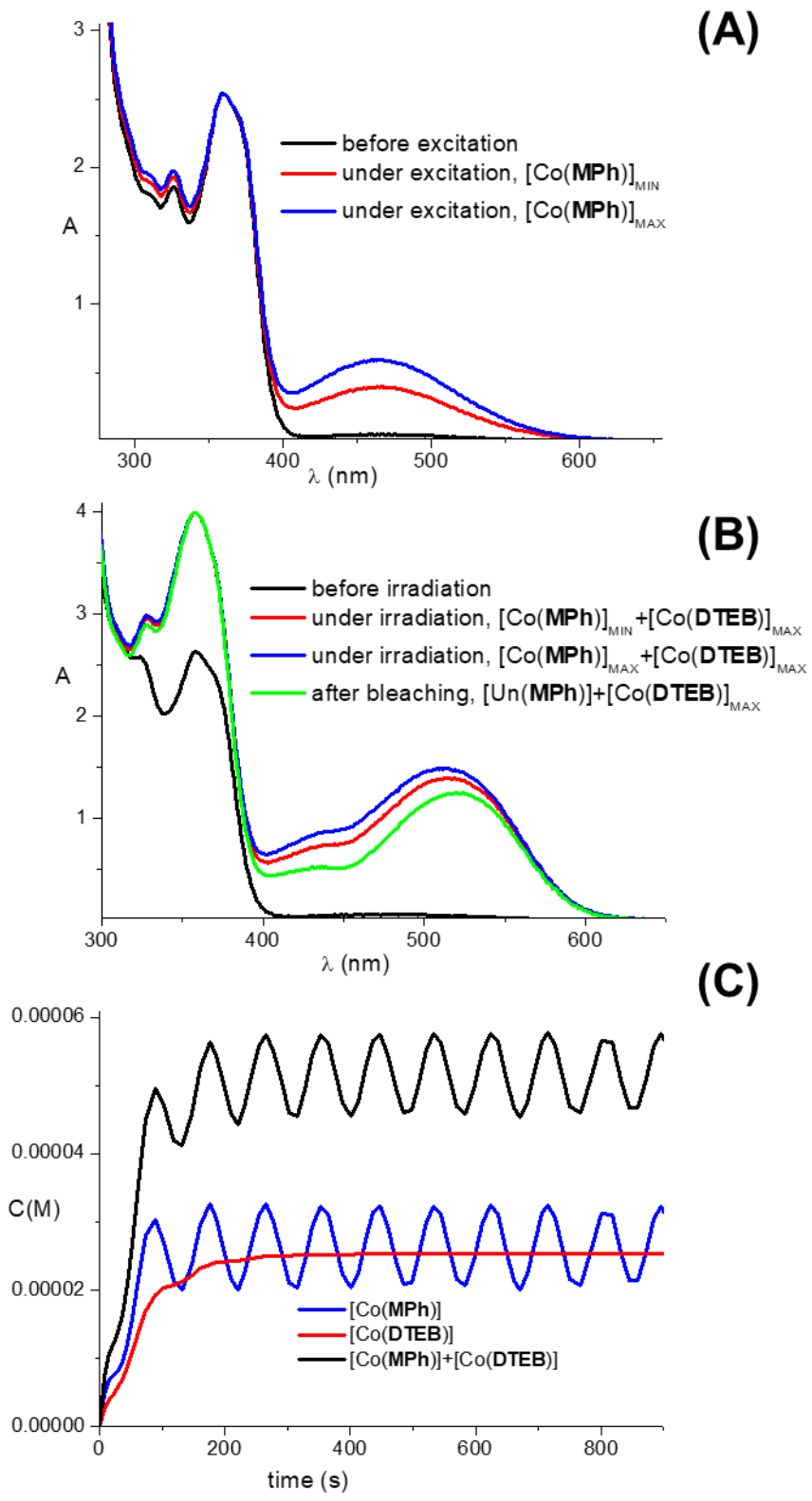

Figure 3. Simulated absorption spectra of **MPh** alone in (A); simulated spectra of **MPh**+**DTEB** in (B); calculated trends of Co(**MPh**) and Co(**DTEB**) concentrations upon oscillatory UV excitation in

(C). For the mathematical details of the simulations and the experimental data see paragraphs 4a and 4b in the SI.

Now, if the solution containing **MPh** and Co(**DTEB**) is irradiated by visible wavelengths included between 400 and 600 nm, the solution bleaches. In other words, the absorption properties of the system containing **DTEB** depend on how much intensity of the UV and visible radiation has interacted with it. **DTEB** works as if it were a memristor. A memristor [36] is an electronic component whose resistance is not constant but depends on how much electric charge has flowed in what direction through it in the past. A memristor remembers its history, and it is used in the field of neuromorphic engineering that trusts in electronic circuits to implement memory effects. When the electric power supply is turned off, the memristor remembers its most recent resistance until it is turned on, again. The same does **DTEB** but regarding absorbance values.

Azo is another photo-reversible photochromic compound that can be used to implement memory effects. Figure 4 reports its simulated memory action. The black trace of Figure 4A is the calculated absorption spectrum of Un(**MPh**) ($4x10^{-5}$ M) and *Trans*(**Azo**) ($4x10^{-5}$ M). If such system receives a periodic UV signal (at 320 nm) transmitted by a **BZ** reaction, the concentrations of Co(**MPh**) starts to oscillate (see the blue trace in Figure 4B), whereas that of *Cis*(**Azo**) grows exponentially (see red trace in Figure 4B) to reach a photo-stationary state. Of course, the sum [Co(**MPh**)]+[*Cis*(**Azo**)] oscillates (see the black trace in Figure 4B). When the concentration of *Cis*(**Azo**) is stationary, the spectra of the overall system oscillates in the range delimited by the blue and the red traces of Figure 4A. When **BZ** interrupts the transmission of its excitatory UV signal, Co(**MPh**) disappears thermally in about one minute, whereas *Cis*(**Azo**) lasts much longer (in fact, for *Cis*(**Azo**) $k_{\Delta} = 0.00000228s^{-1}$ [37]), retaining the information regarding the last UV excitation for about one week. Such information is coded in the profile of the absorption spectrum represented by the green trace of Figure 4A. With respect to the original black trace, the green spectrum shows much smaller absorbance values in the

UV and slightly larger values in the visible region included between 400 and 525 nm. The transformation of *Trans*(**Azo**) to *Cis*(**Azo**) determines a significant long-term depression (LTD) of absorbance in the UV between 280 and 350 nm and a tiny long-term potentiation (LTP) of absorbance in the visible between 400 and 500 nm (see also paragraphs 4c and 4d in SI for the details of the simulations and the experimental results).

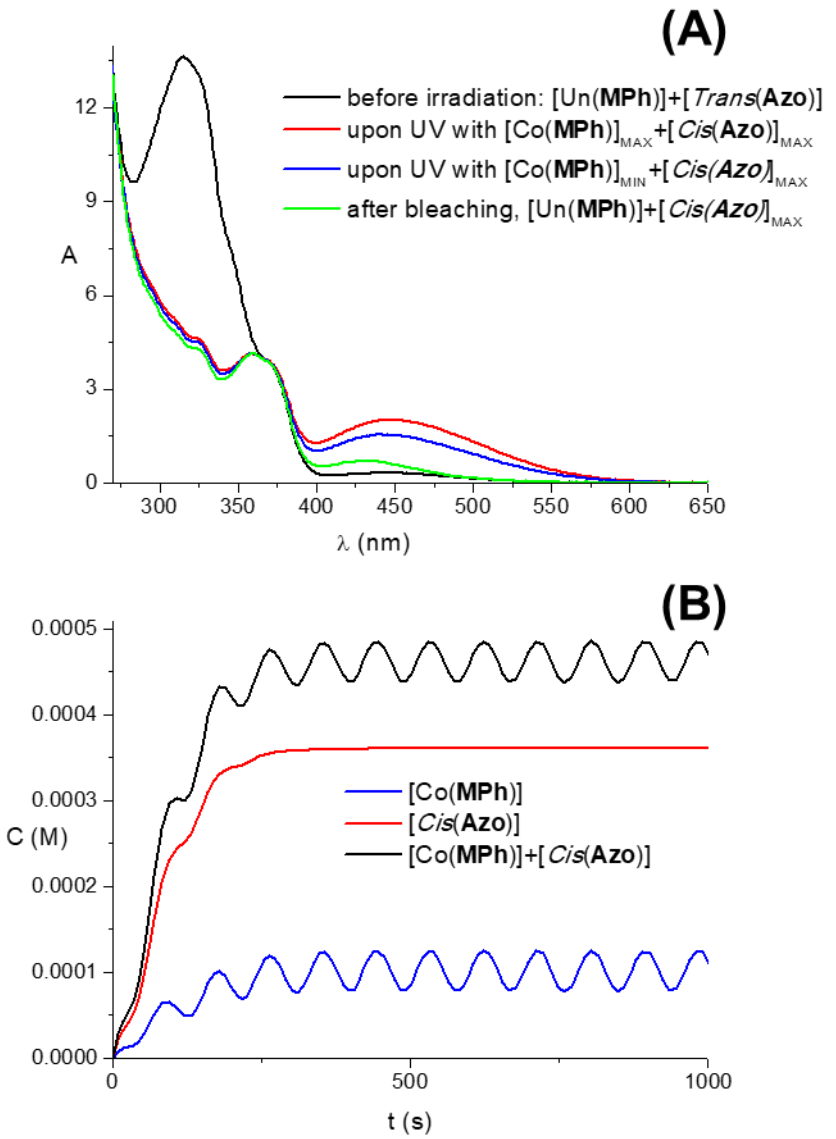

Figure 4. Simulated absorption spectra of **MPh**+**Azo** in (A); calculated trends of Co(**MPh**) and *Cis*(**Azo**) concentrations upon oscillatory UV excitation in (B). For the mathematical details of the simulations and the experimental data see paragraphs 4c and 4d in SI.

The different properties of **DTEB** and **Azo** allow implementing memory effects having distinct spectral features and durability. The durability is infinite with **DTEB** but shorter with **Azo**.

Communication of a chaotic signal

Chaotic neurons are widespread in the nervous system because the instability inherent in their nonlinear dynamics facilitates the extraordinary ability of neural networks to adapt, store and create information [15]. Herein, we propose the use of hydrodynamic photochemical oscillators [38] as dynamic models of chaotic neurons. A Hydrodynamic Photochemical Oscillator (**HPO**) consists of a solution of a direct thermally reversible photochromic compound. The photochromic solution is UV-irradiated not uniformly but only at the bottom of the cuvette (see graph (0) in Figure 5). The UV irradiation generates the colored form and simultaneously warms the solution in the lower part of the cuvette. The solution is maintained in an uncapped cuvette. The partial evaporation of the solvent induces a cooling effect at the top of the solution. A vertical thermal gradient of the order of tenths of degrees Kelvin, which is stationary within the time range of the experiments, promotes convective motion of the fluid. Pictures of the convective motion in action and an accurate analysis of the physical-chemistry of the **HPO**s have been published in the reference [38]. The hydrodynamic convective flow of the solvent, combined with the thermally reversible photochromism, generates color hydrodynamic waves and aperiodic oscillations of the transmittance values in both the visible and UV regions. The **HPO** gives rise to spectrophotometric time series that have been demonstrated to be chaotic [39-41]. In this work, we have used an **HPO** based on **MPh**. Some representative transmittance spectra are reported in graph (1) of Figure 5. The green trace has been recorded before UV irradiation, whereas the red, blue and black traces are three examples of transmittance spectra collected at different delay times after the beginning of the irradiation and the convective motion of the solvent acetone. The latter three spectra demonstrate that **HPO(MPh)** originates appreciable

transmittance oscillations especially in the violet-blue region of the visible spectrum. These oscillations are aperiodic as shown in graph (3) of Figure 5, which reports the trend of transmittance at 464 nm over time. When **HPO(MPh)** is irradiated by continuous UV and violet-blue radiation, it transmits an aperiodic signal that is particularly intense in the violet-blue region. Such optical signal has been sent to another cuvette containing 1 mL of the strongly fluorescent **C_8Ac** solved in acetonitrile. The solution of **C_8Ac** is entirely under irradiation. The aperiodic violet-blue light transmitted by **HPO(MPh)** excites **C_8Ac** (see the gray absorption spectrum in graph (2) of Figure 5). **C_8Ac** emits green fluorescence (see the green spectrum in graph (2) of Figure 5). The emission intensity of **C_8Ac** is directly proportional to the violet-blue transmittance of **HPO(MPh).** In fact, the red, blue and black emission spectra of **C_8Ac**, appearing in graph (2), have been collected when the red, blue and black transmittance spectra, appearing in graph (1), have been recorded for **HPO(MPh)**. **C_8Ac** synchronizes with **HPO(MPh)**. **C_8Ac** behaves like a phasic photo-excitable neuron model as photochromic compounds do. Since **C_8Ac** recovers its ground state very fast, in a few nanoseconds, it synchronizes perfectly in phase with **HPO(MPh)**. The green luminescence of **C_8Ac** is aperiodic as the visible light transmitted by **HPO(MPh)** (compare graphs (3) and (4) of Figure 5).

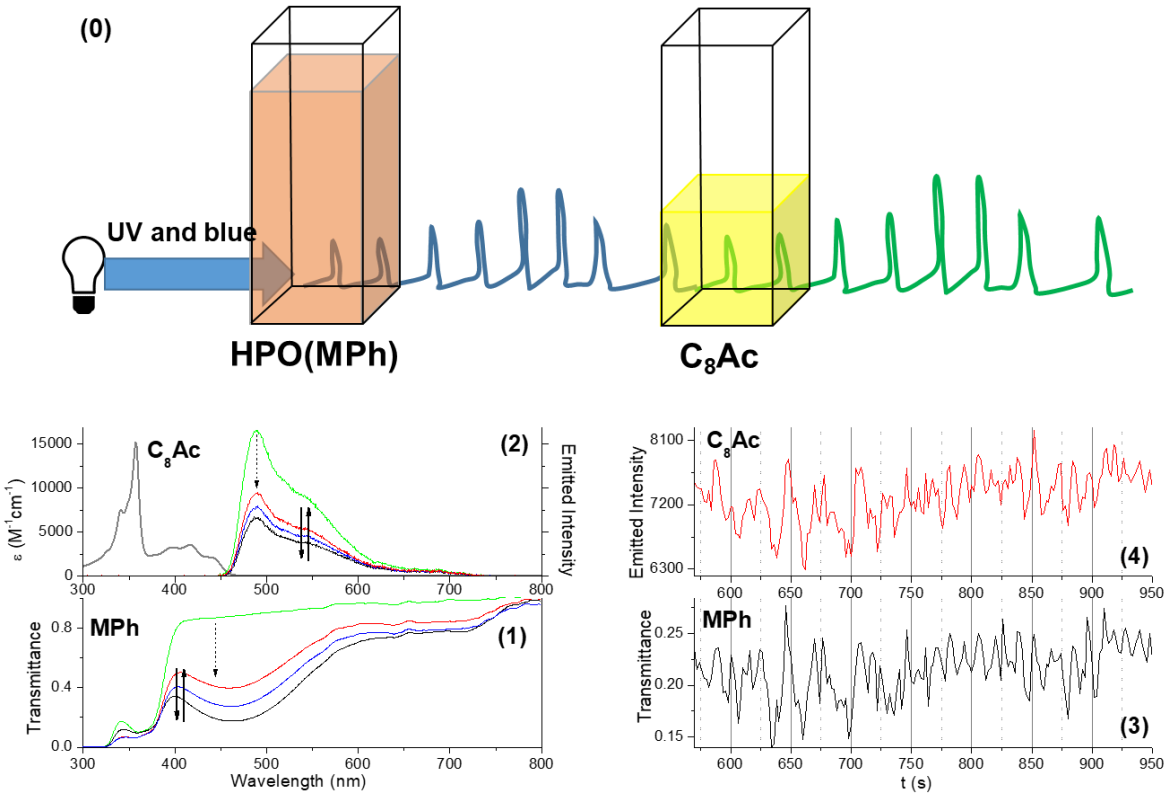

Figure 5. Scheme of the optical communication between **HPO(MPh)** and **C8Ac** in (0), wherein **HPO(MPh)** is irradiated by UV-visible frequencies and transmits an aperiodic signal to **C8Ac**. Spectral evolution in transmittance for **HPO(MPh)** (with [**MPh**]=7.9x10^{-5} M in acetone) (1), and in emission for **C8Ac** (with [**C8Ac**]=0.01 M in acetonitrile) (2). In (2), the gray trace is the absorption spectrum of **C8Ac**. Profiles of the intensity transmitted by **HPO(MPh)** at 464 mm (3) and the intensity emitted by **C8Ac** at 488 nm (4).

The analysis of the aperiodic spectrophotometric signal transmitted by **HPO(MPh)** reveals that it is chaotic. Chaos should not be mistaken for noise, as the former has a phase-space structure which can be utilized for synchronization, transmission of information, and regularization of the neural networks for the performance of critical functions. The phase space for the time series generated by **HPO(MPh)** has four as the time delay (τ) and six as the embedding dimension (m) (see the Experimental paragraph for more information). After plotting the **HPO(MPh)** time series in its six-dimensional phase space,

we obtain a positive Lyapunov exponent (λ=0.042) and a fractal correlation dimension (*D*=9.2) for its attractor (see paragraph 5 of SI for the details). The strong coupling between the transmitter **HPO(MPh)** and receiver **C₈Ac** is proved by the features of the aperiodic luminescence signal emitted by **C₈Ac**. In fact, after applying the Takens' theorem, we define a phase space for **C₈Ac**, which has the same time delay (τ=4) and the same number of embedding dimensions (*m*=6) of that built for the time series generated by **HPO(MPh).** Moreover, we find that even the **C₈Ac** time series has chaotic features with a positive Lyapunov exponent and a fractal correlation dimension, which are very similar to those of **HPO(MPh)**, as shown in Table 1.

Table 1. Time delay (τ), embedding dimension (m), largest Lyapunov exponent (λ) and correlation dimension (D) of the strange attractors determined for the time series of the blue light transmitted by **HPO(MPh)** and the green light emitted by **C₈Ac**. The data for the calculation of these parameters are reported in paragraph 5 of the SI.

Signal	**τ**	**m**	**λ**	**D**
HPO(MPh)	4	6	0.042	9.2
C₈Ac	4	6	0.039	8.5

The quality of the communication of the chaotic signal depends on the synchronization between **HPO(MPh)** and **C₈Ac**, as shown in Figure 6. The upper graph reports the normalized signal of the receiver (nS_R) vs. that of the transmitter (nS_T). The data points stay quite close to the bisector, demonstrating a good synchronization. The deviations from the bisector are mainly due to the noise of the detectors used to record both nS_T and nS_R. The lower graph of Figure 6 reports the trend of the logarithm of the absolute value of the difference $nS_T - nS_R$ in the time range [570 – 950] s. This

experiment is the first example of good transmission of a chaotic optical signal between two fluid chemical systems.

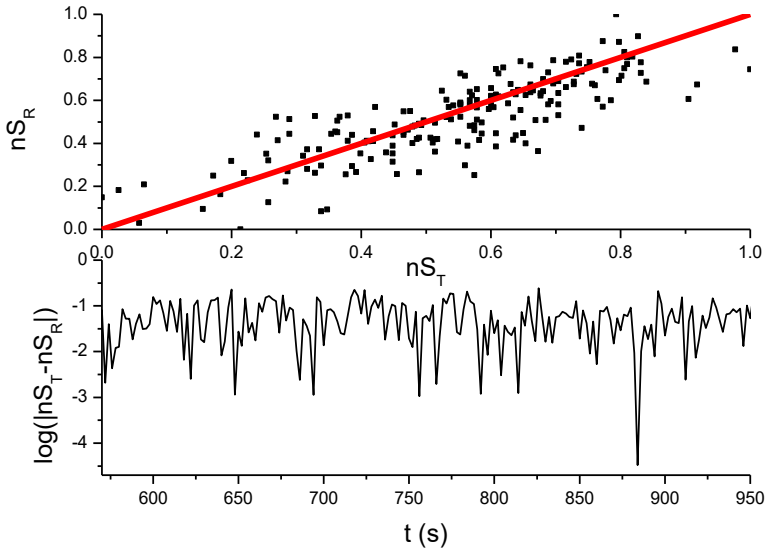

Figure 6. The upper graph shows the trend of the normalized Signal of the Receiver (nS_R) vs. the normalized Signal of the Transmitter (nS_T) in the time range [570 – 950] s. The lower graph reports the logarithm of the absolute value of the difference between the two signals: $nS_T - nS_R$.

Conclusions

This work is an essential contribution to the development of neuromorphic engineering based on solutions of nonlinear chemical systems. In fact, it presents some significant achievements.

First of all, it shows that thermally reversible (T-type) photochromic and luminescent compounds are dynamic models of "phasic" excitable neurons. The thermally reversible photochromic materials synchronize out-of-phase with the transmitter of an excitatory signal (for instance, the **BZ** reaction transmitting a periodic UV signal). On the other hand, luminescent compounds, such as **C_8Ac**, synchronize in phase. The different type of synchronization depends on the relaxation time of the

excitable neuron model. When the relaxation time is short if compared with the period of the excitatory signal, the synchronization is in phase; if it is comparable or longer than the period of the oscillations, the synchronization is out-phase. In the latter case, the longer the relaxation time, the more significant the phase shift ($\Delta\theta$) between the transmitter and the receiver.

Second, the natural spectral evolution of a photochromic compound that transforms from the uncoloured to the coloured form can generate either a positive or a negative feedback action in the communication of optical signals. The optical feedback actions of photochromic compounds are both "self" and "not-self". This kind of feedback actions is wavelength-dependent. This consideration demonstrates that the optical communication can rely upon such wealthy code as it is the UV and visible radiation.

Third, photo-reversible (P-type) photochromic compounds are useful for the implementation of adjustable, analog and non-volatile optical synaptic connections. Therefore, compounds such as **DTEB** and **Azo** allow implementing memory effects.

Fourth, Hydrodynamic Photochemical Oscillators can be used as dynamic models of chaotic neurons to transmit chaotic signals.

We are now designing new systems for the optical communication among more than two elements with the purpose of imitating the dynamic behavior of real neural networks.

Acknowledgements

Authors acknowledge the financial support by the University of Perugia, Fondo Ricerca di Base 2014, D. D. n. 170, 23/12/2014.

References

[1] Russell SJ, Norvig P. Artificial Intelligence. A Modern Approach. Prentice-Hall, New Jersey; 1995.

[2] Mead C. Analog VLSI and Neural Systems. Addison-Wesley, MA; 1989.

[3] Donoghue JP. Bridging the Brain to the World: A Perspective on Neural Interface Systems Neuron. 2008; 60: 511-521.

[4] Service RF. The brain chip. Science 2014; 345: 614-616.

[5] Merolla PA, Arthur JV, Alvarez-Icaza R, Cassidy AS, Sawada J, Akopyan F, Jackson BL, Imam N, Guo C, Nakamura Y, Brezzo B, Vo I, Esser SK, Appuswamy R, Taba B, Amir A, Flickner MD, Risk WP, Manohar R, Modha DS. A million spiking-neuron integrated circuit with a scalable communication network and interface. Science 2014; 345: 668-673.

[6] Ha SD, Ramanathan S. Adaptive oxide electronics: A review. J. Appl. Phys. 2011; 110: 071101.

[7] Di Ventra M, Pershin YV. The parallel approach. Nat. Phys. 2013; 9: 200-202.

[8] Pilarczyk K, Podborska A, Lis M, Kawa M, Migdal D, Szacilowski K. Synaptic Behavior in an Optoelectronic Device Based on Semiconductor-Nanotube Hybrid. Adv. Electron. Mater. 2016; 1500471.

[9] Tuma T, Pantazi A, Le Gallo M, Sebastian A, Eleftheriou E. Stochastic phase-change neurons. Nat. Nanotechnol., 2016; 11: 693-699.

[10] Gentili PL. A strategy to face complexity: The development of chemical artificial intelligence. Communications in Computer and Information Science. 2017; 708: 151-160. Editors Rossi F, Piotto S, Concilio S, Springer International Publishing.

[11] Gentili PL. Small steps towards the development of chemical artificial intelligent systems. RSC Advances 2013; 3: 25523-25549.

[12] Gentili PL, Horvath V, Vanag VK, Epstein IR. Belousov-Zhabotinsky "chemical neuron" as a binary and fuzzy logic processor. Int. J. Unconv. Comput. 2012; 8: 177-192.

[13] Pina F, Melo MJ, Maestri M, Passaniti P, Balzani V. Artificial Chemical Systems Capable of Mimicking Some Elementary Properties of Neurons. J. Am. Chem. Soc. 2000; 122: 4496-4498.

[14] Izhikevich EM. Dynamical Systems in Neuroscience. MIT Press: Cambridge; 2007.

[15] Rabinovich MI, Varona P, Selverston AI, Abarbanel HDI. Dynamical principles in neuroscience. Rev. Mod. Phys. 2006; 78: 1213-1265.

[16] Marek M, Stuchl I. Synchronization in two interacting oscillatory systems. Biophys. Chem. 1975; 3: 241-248.

[17] Hohmann W, Kraus M, Schneider FW. Pattern Recognition by Electrical Coupling of Eight Chemical Reactors. J. Phys. Chem. A 1999; 103: 7606-7611.

[18] Zlotnik A, Nagao R, Kiss IZ, Li Jr-S. Phase-selective entrainment of nonlinear oscillator ensembles. Nat. Commun. 2016; 7: 10788.

[19] Taylor AF, Tinsley MR, Showalter K. Insights into collective cell behaviour from populations of coupled chemical oscillators. Phys. Chem. Chem. Phys. 2015; 17: 20047-20055.

[20] Horvath V, Gentili PL, Vanag VK, Epstein IR. Pulse-Coupled Chemical Oscillators with Time Delay. Angew. Chem. Int. Ed. 2012; 51: 6878-6881.

[21] Szacilowski K. Molecular Logic Gates Based on Pentacyanoferrate Complexes: From Simple Gates to Three-Dimensional Logic Systems. Chem. Eur. J. 2004; 10: 2520-2528.

[22] Raymo F. M., Tomasulo M. Optical Processing with Photochromic Switches. Chem. Eur. J. 2006; 12: 3186-3193.

[23] Gentili PL, Giubila MS, Germani R, Romani A, Nicoziani A, Spalletti A, Heron BM. Optical Communication among Oscillatory Reactions and Photo-Excitable Systems: UV and Visible Radiation Can Synchronize Artificial Neuron Models. Angew. Chem. Int. Ed. 2017; 56: 7535-7540.

[24] Gentili PL, Rightler AL, Heron BM, Gabbutt CD. Extending human perception of electromagnetic radiation to the UV region through biologically inspired photochromic fuzzy logic (BIPFUL) systems. Chem. Commun. 2016; 52: 1474-1477.

[25] Hanazawa M, Sumiya R, Horikawa Y, Irie M. Thermally irreversible photochromic systems. Reversible photocyclization of 1,2-bis (2-methylbenzo[b]thiophen-3-yl)perfluorocyclocalkene derivatives. J. Chem. Soc. Chem. Commun. 1992; 3: 206-207.

[26] Hegger R, Kantz H, Schreiber T. Practical implementation of nonlinear time series methods: The TISEAN package. Chaos 1999; *9*: 413-435.

[27] Takens F. Dynamical Systems and Turbulence. Eds. Rand DA, Young LS. Springer, Berlin, 1981.

[28] Fraser AM, Swinney HL. Independent coordinates for strange attractors from mutual information. Phys. Rev. A 1986; 33: 1134-1140.

[29] Kennel MB, Brown R, Abarbanel HDI. Determining embedding dimension for phase-space reconstruction using a geometrical construction. Phys. Rev. A 1992; 45: 3403-3411.

[30] Rosenstein MT, Collins JJ, De Luca CJ. A practical method for calculating largest Lyapunov exponents from small data sets. Physica D 1993; 65: 117-134.

[31] Grassberger P, Procaccia I. Characterization of Strange Attractors. Phys. Rev. Lett. 1983; 50: 346-349.

[32] Ramirez J-M, Tryba AK, Peña F. Pacemaker neurons and neuronal networks: an integrative view. Curr Opin Neurobiol. 2004; 14: 665-674.

[33] Meng X, Huguet G, Rinzel J. Type III Excitability, Slope Sensitivity and Coincidence Detection. Discrete Contin. Dyn. Syst. Ser. A. 2012; 32: 2729-2757.

[34] Prescott SA. Excitability: Types I, II and III. In Encyclopedia of Computational Neuroscience, Jaeger D, Jung R, (Eds), pp. 1-7, Springer Science 2015.

[35] Korn H, Faure P. Is there chaos in the brain? II. Experimental evidence and related models. C. R. Biologies 2003; 326: 787–840.

[36] Yang JJ, Strukov DB, Stewart DR. Memristive devices for computing. Nat. Nanotechnol. 2013; 8: 13-24.

[37] Bandara HMD, Burdette SC. Photoisomerization in different classes of azobenzene. Chem. Soc. Rev. 2012; 41: 1809-1825.

[38] Gentili PL, Dolnik M, Epstein IR. "Photochemical Oscillator": Colored Hydrodynamic Oscillations and Waves in a Photochromic System. J. Phys. Chem. C 2014, 118: 598-608.

[39] Gentili PL, Gotoda H, Dolnik M, Epstein IR. Analysis and prediction of aperiodic hydrodynamic oscillatory time series by feed-forward neural networks, fuzzy logic, and a local nonlinear predictor. Chaos 2015, 25, 013104-1 - 013104-14.

[40] Hayashi K, Gotoda H, Gentili PL. Probing and exploiting the chaotic dynamics of a hydrodynamic photochemical oscillator to implement all the basic binary logic functions. Chaos 2016, 26, 053102-1-053102-8.

[41] Gentili PL, Giubila MS, Heron BM. Processing Binary and Fuzzy Logic by Chaotic Time Series Generated by a Hydrodynamic Photochemical Oscillator. ChemPhysChem 2017, 18, 1831-1841.